THE JOURNAL OF PHYSICAL CHEMISTRY B

Article

Cite This: J. Phys. Chem. B 2019, 123, 2853−2863

pubs.acs.org/JPCB

Monitoring the Structure-Dependent Reaction Pathways of Guanine Radical Cations in Triplex DNA: Deprotonation Versus Hydration

Yinghui Wang,[†,§] Hongmei Zhao,[†] Qian Zhou,[‡] Xiaojuan Dai,[‡] Kunhui Liu,[‡] Di Song,[†] and Hongmei Su*[,‡]

[†]Beijing National Laboratory for Molecular Science, Institute of Chemistry, Chinese Academy of Sciences, Beijing 100190, China

[‡]College of Chemistry, Beijing Normal University, Beijing 100875, China

[§]University of Chinese Academy of Sciences, Beijing 100049, China

Supporting Information

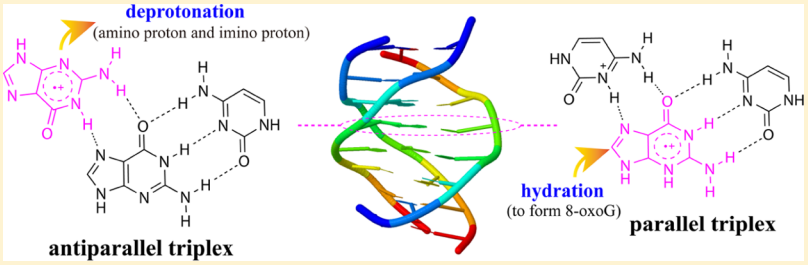

ABSTRACT: Exposure of DNA to one-electron oxidants leads initially to the formation of guanine radical cations ($G^{\bullet+}$), which may degrade by deprotonation or hydration and ultimately cause strand breaks or 8-oxoG lesions. As the structure is dramatically changed by binding of the third strand in the major groove of the target duplex, it makes the triplex an interesting DNA structure to be examined and compared with the duplex on the $G^{\bullet+}$ degradation pathways. Here, we report for the first time the time-resolved spectroscopy study on the $G^{\bullet+}$ reaction dynamics in triplex DNA together with the Fourier transform infrared characterization of steady-state products, from which structural effects on the reactivity of $G^{\bullet+}$ are unraveled. For an antiparallel triplex-containing GGC motif, $G^{\bullet+}$ mainly suffers from fast deprotonation $(9.8 \pm 0.2) \times 10^6$ s^{-1}, featuring release of both N_1−H and N_2−H of G in the third strand directly into bulk water. The much faster and distinct deprotonation behavior compared to the duplex should be related to long-resident water spines in the third strand. The $G^{\bullet+}$ hydration product 8-oxoG is negligible for an antiparallel triplex; instead, the 5-HOO−(G−H) hydroperoxide formed after $G^{\bullet+}$ deprotonation is identified by its vibrational marker band. In contrast, in a parallel triplex (C^+GC), the deprotonation of $G^{\bullet+}$ occurs slowly $(6.0 \pm 0.3) \times 10^5$ s^{-1} with the release of N_1−H, while $G^{\bullet+}$ hydration becomes the major pathway with yields of 8-oxoG larger than in the duplex. The increased positive charge brought by the third strand makes the G radical in the parallel triplex sustain more cation character and prone for hydration. These results indicate that non-B DNA (triplex) plays an important role in DNA damage formation and provide mechanistic insights to rationalize why triplex structures might become hot spots for mutagenesis.

INTRODUCTION

One-electron oxidation of DNA is one of the main causes of cytotoxic DNA lesions related to mutagenesis, apoptosis, or cancer.[1,2] In particular, one-electron oxidation initially generates a radical cation (hole) that can migrate through DNA strands and ultimately end up selectively at the sites of guanine (G) because G is the most easily oxidized nucleobase.[3−6] Subsequently, the radical cation ($G^{\bullet+}$) undergoes decay by additional reactions, mainly deprotonation and hydration, to generate various lesion products.[7−12] $G^{\bullet+}$ deprotonates to form a guanine neutral radical $G(-H)^{\bullet}$,[13−15] which would then react with dioxygen O_2 and lead to imidazolone (Iz) and oxazolone (Oz) (Scheme 1).[16−18] Both Iz and Oz are alkali-labile products, which may be completely converted to strand breaks.[19,20] Meanwhile, the hydration of $G^{\bullet+}$ results in the formation of 7,8-dihydro-8-oxoguanine (8-oxoG), one of the most important products related to "oxidation stress" in biological systems (Scheme 1).[21,22] If not removed, 8-oxoG might induce G:C to T:A transversion during replication by pairing with adenine, which is often found in the coding sequences of oncogenes and tumor suppressor genes.[23,24]

The degradation pathway of $G^{\bullet+}$ that dictates the type of DNA damage, interestingly, is found to be strongly structure-dependent.[7−9,21] In a G-base monomer or in single-stranded DNA (ssDNA), $G^{\bullet+}$ mainly undergoes deprotonation by loss of the imino proton (N_1−H) in neutral solutions with a rate constant of $\sim 10^7$ s^{-1},[13] whereas the hydration of $G^{\bullet+}$ $(3.0 \times 10^2$ $s^{-1})$ is too slow to compete.[25] This type of $G^{\bullet+}$ degradation is considered to make the strand breaks familiar in ssDNA.

Received: January 21, 2019
Revised: March 5, 2019
Published: March 5, 2019

DOI: 10.1021/acs.jpcb.9b00608
J. Phys. Chem. B 2019, 123, 2853−2863

Scheme 1. (a) Degradation Pathways of $G^{\bullet+}$ in the Free Base dG and (b) Two Deprotonation Pathways of $G^{\bullet+}$

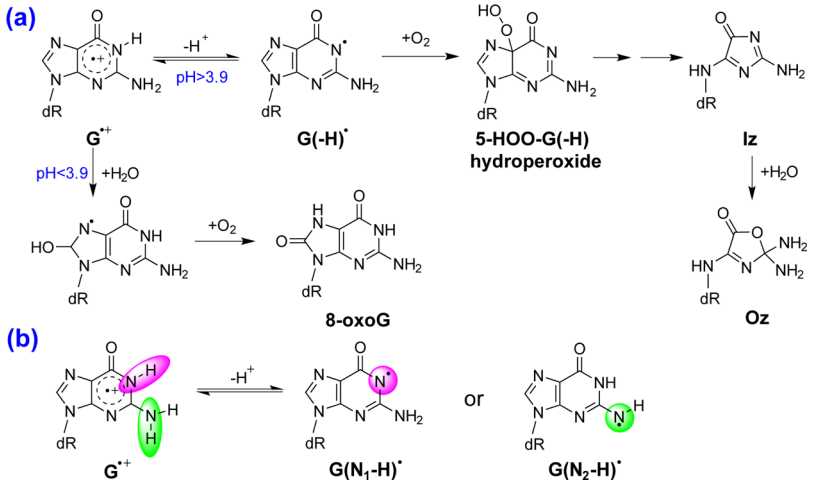

Scheme 2. (a) Base Pairs of C^+GC in the Parallel Triplex and GGC in the Antiparallel Triplex; (b) sequence of the Target Duplex and the Antiparallel and Parallel Triplex as Well as Their Folding Style

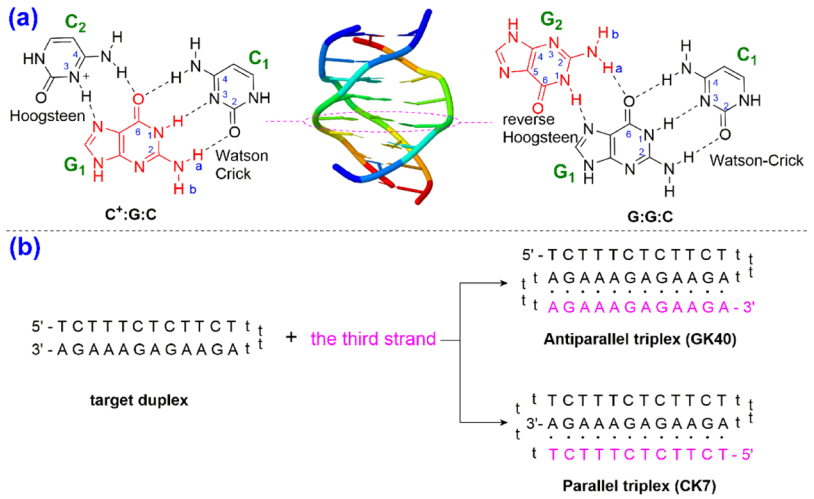

Only in acidic solution pH (2.5) when the deprotonation is suppressed can $G^{\bullet+}$ be hydrated to generate 8-oxoG.[25] Different from ssDNA, the G base in double-strand DNA (dsDNA) is paired with cytosine through Watson−Crick hydrogen bonding. The deprotonation occurs along the central hydrogen bond in dsDNA, where the N_1 proton of $G^{\bullet+}$ partially transfers to N_3 of C in the base pair, as the protonation pK_a of N_3 in C (4.3) is slightly higher than the deprotonation pK_a of N_1 in $G^{\bullet+}$ (3.9), and then, the proton is eventually released into the solvent.[13,14] Essentially, the chemical equilibrium $[G(-H)^{\bullet}{:}H^+C \leftrightarrows G^{\bullet+}{:}C]$ within the base pair diminishes the probability of escape of the proton, allowing the $G(-H)^{\bullet}$ radicals to retain some cationic character in dsDNA. The hydration of $G^{\bullet+}$ can thus compete with the release of the proton into bulk solution and ultimately leads to the formation of high-yield 8-oxoG, which is ∼7 greater than in ssDNA.[21]

Compared to the sophisticated studies devoted to dsDNA, much less is known for the radical cation degradation behavior of $G^{\bullet+}$ in triplex DNA that has an entirely different structure. As an important non-B-form DNA structure in cells, triplex formation might adversely affect DNA replication and is associated with a number of inherited as well as acquired human diseases.[26−29] Triplex is a family of triple helical structures formed when a single-stranded triplex-forming oligonucleotide binds in the major groove of target duplex DNA by Hoogsteen (parallel triplex) or reverse Hoogsteen hydrogen bonding (antiparallel triplex) as shown in Scheme 2.[30−32] Structural studies have revealed that the binding of the third strand into the target duplex changes the hydrogen bonding, solvent accessibility, and base stacking.[33−39] On the basis of the structural features, the $G^{\bullet+}$ degradation in triplex DNA is anticipated to be different from single-strand and duplex DNA.

Saito and his co-workers reported that the oxidative DNA cleavage occurred exclusively at G-repeat sequences in the third strand of the antiparallel GGC-type triplex, meaning that triplex DNA can serve as an effective hole trap.[40] However, irradiation of the parallel triplex DNA linked with anthraquinone leads to strand breaks at remote GG sequences, indicating that the C^+GC-type triplex blocks the hole trap and facilities hole migration.[41] In general, the strand breaks are linked to $G^{\bullet+}$ deprotonation. Therefore, these studies based on steady-state measurements actually point to the different reaction properties of $G^{\bullet+}$ within the two types of the triplex DNA structure. Obviously, the distinct structural features of

DOI: 10.1021/acs.jpcb.9b00608
J. Phys. Chem. B 2019, 123, 2853−2863

triplex DNA make it an interesting candidate to be examined and compared with duplex DNA, from which the structural effects on the reactivity of $G^{\bullet+}$ can be unraveled. Furthermore, triplex DNA structures are postulated to be responsible for some oxidative breakpoint hotspots that may induce the genomic instability.[42,43] Thus, research on $G^{\bullet+}$ degradation in triplex DNA also has biological significance.

In this context, we combined the time-resolved UV−vis absorption and Fourier transform infrared (FTIR) spectroscopy to monitor the structure-dependent degradation pathways of $G^{\bullet+}$ in antiparallel and parallel triplex DNA, respectively. For the first time, the distinct $G^{\bullet+}$ degradation pathways in the antiparallel and parallel triplex in comparison with the duplex are disclosed. For the antiparallel triplex, $G^{\bullet+}$ mainly suffers from fast deprotonation $(9.8 \pm 0.2) \times 10^6\ s^{-1}$, featuring release of both imino N_1−H and exocyclic amino N_2−H of G in the third strand directly into bulk water. The unique deprotonation behavior should be related to the presence of the long-resident water spines in the groove of the triplex. The 5-HOO−(G−H) hydroperoxide formed after $G^{\bullet+}$ deprotonation is identified in the IR spectra, providing spectral evidence for the existence of this crucial precursor of Iz and Oz lesions. In contrast, in the parallel triplex, the deprotonation of $G^{\bullet+}$ occurs slowly $(6.0 \pm 0.3) \times 10^5\ s^{-1}$ with the release of N_1−H, while $G^{\bullet+}$ hydration becomes the major pathway with yields of 8-oxoG larger than in duplex DNA. The increased positive charge brought by the third strand makes the G radical in the parallel triplex sustain more cation character and prone for hydration. The degradation pathways of $G^{\bullet+}$ indicate that the parallel triplex may mainly suffer from 8-oxoG damage because of the prone hydration of $G^{\bullet+}$, while the fast $G^{\bullet+}$ deprotonation in the antiparallel triplex can be converted to another lesion type of strand breaks. These results reveal the significant role of the DNA structure in governing $G^{\bullet+}$ reaction dynamics and provide mechanistic insights for understanding why the genomic regions with the propensity to fold transiently into non-B DNA secondary structures might become hot spots for mutagenesis.

MATERIALS AND METHODS

Materials. Sodium persulfate was purchased from Sigma. Sodium phosphate buffers in H_2O and D_2O were purchased from Beijing Solarbio Science & Technology Co., Ltd. The DNA oligonucleotides GK40, CK7, and target dsDNA (Scheme 2) were purchased from Sangon Biotech (shanghai) Co., Ltd. in a form purified by high-performance liquid chromatography/polyacrylamide gel electrophoresis. Single-strand concentrations were determined by monitoring the absorbance at 260 nm in the UV−vis spectra, and the corresponding extinction coefficients of 446 100, 396 500, and 270 500 $M^{-1}\ cm^{-1}$, respectively, for GK40, CK7, and dsDNA are obtained from www.idtdna.com. The triplex DNAs were prepared as follows. The oligonucleotide samples were dissolved in 100 mM sodium phosphate buffer solution at pH 7.5 for GK40 and the target duplex as well as 100 mM sodium phosphate buffer solution at pH 5.0 for CK7, then incubated at 4 °C overnight. The formation of triplex DNA was confirmed by circular dichroism spectroscopy. All the reagents were used as received.

Circular Dichroism Spectroscopy. Circular dichroism experiments were performed at room temperature using a Jasco-815 spectropolarimeter. Each measurement was recorded from 200 to 320 nm in a 1 cm path length quartz cuvette with a scanning rate of 1000 nm/min. The final data were the average of three measurements. The concentration of triplex DNA is 2.0 μM for GK40, CK7, and dsDNA. The scan of the buffer alone was used as the background, which was subtracted from the average scan for each sample.

Laser Flash Photolysis. Nanosecond time-resolved transient absorption spectra were measured using a nanosecond laser flash photolysis setup Edinburgh LP920 spectrometer (Edinburgh Instruments Ltd.), combined with a Nd:YAG laser (SureliteII, Continuum Inc.). The sample was excited by a 355 nm laser pulse (1 Hz, 10 mJ/pulse, fwhm ≈ 7 ns). The analyzing light was from a 450 W pulsed xenon lamp. A monochromator equipped with a photomultiplier for collecting the spectral range from 300 to 700 nm was used to analyze transient absorption spectra. Data were analyzed by online software of the LP920 spectrophotometer.

Generation of Sulfate Radical Anions. Sulfate radicals anions, $SO_4^{\bullet-}$, were generated by the photodissociation of peroxodisulfate anions ($S_2O_8^{2-}$) by nanosecond 355 nm laser pulses. Here, $Na_2S_2O_8$ is photolyzed as the $SO_4^{\bullet-}$ precursor.

$$S_2O_8^{2-} + h\nu \rightarrow 2SO_4^{\bullet-}$$

The sulfate radical $SO_4^{\bullet-}$ shows transient absorption with the resolved band at 450 nm, which is in good agreement with the spectra reported previously.[15] The photodissociation of $S_2O_8^{2-}$ is rapid, and all $SO_4^{\bullet-}$ are generated within the ∼7 ns laser pulse duration. The concentration of $SO_4^{\bullet-}$ can be estimated by the absorbance at 450 nm using an extinction coefficient of 1600 $M^{-1}\ cm^{-1}$, which is 7.2 μM and much smaller than the concentration of G in triplex DNA (at least 250 μM triplex concentration). With the triplex DNA in large excess, the bimolecular reaction of $SO_4^{\bullet-}$ oxidizing triplex DNA becomes a pseudo-first-order reaction. The 355 nm photolysis of the triplex alone does not generate any signal, providing a neat background for the detection of the reactions of $SO_4^{\bullet-}$ with DNA.

FTIR Spectroscopy. FTIR spectra were recorded using a Nicolet Nexus 870 FTIR spectrometer. The samples were injected in an IR cell with 2 mm thick CaF_2 windows (path length, 100 μm) and excited by a 355 nm laser pulse (1 Hz, 10 mJ/pulse, fwhm ≈ 7 ns). The laser excitation beam was directed through an iris aperture (3 mm in diameter) and overlapped with the infrared beam in the sample cell. The IR spectra were collected with a spectral resolution of 8 cm^{-1}.

Theoretical Calculation Methods. The ground-state geometries and vibrational frequencies were calculated by using the density functional theory at the B3LYP/6-31++G(d,p) level, which is usually a sufficient computational method for the current system.[44,45] The solvent effects were simulated with the polarized continuum model (PCM) or under the solvent model which includes seven explicit water molecules (D_2O) combined with a PCM approach. The calculations were all performed with the Gaussian 09 program package.[46]

RESULTS AND DISCUSSION

Triplex DNA Structure Formation. We choose the oligonucleotide sequences GK40 and CK7 containing pyrimidine−purine−purine segments and pyrimidine−purine−pyrimidine segments, respectively. These two sequences can fold back twice on themselves and form an intramolecular triplex in which the third strand would adopt an antiparallel

DOI: 10.1021/acs.jpcb.9b00608
J. Phys. Chem. B 2019, 123, 2853−2863

orientation or a parallel orientation with respect to the homologous purine strand of the target duplex as shown in Scheme 2. Specifically, in the pH 7.5 sodium phosphate buffer solution, the 3′ terminal purine segment of GK40 folds back via the tttt loop and pairs with the homologous purine strand of the target duplex by the reversed Hoogsteen hydrogen bonds, forming the antiparallel triplex with GGC and AAT motifs. For CK7, the 5′ terminal pyrimidine segments (C base) are partially protonated in the pH 5.0 sodium phosphate buffer solution and can fold back to pair with the homologous purine strand of the target duplex by Hoogsteen hydrogen bonds, forming the parallel triplex with C^+GC and TAT motifs. Fujimoto and his co-workers reported that for the antiparallel triplex (GK40), the CD spectra displayed two positive bands (280 and 223 nm) and one negative band (248 nm) and the 223 nm positive band had increased intensity than the target duplex. For parallel triplex DNA (CK7), the positive band at 280 nm and the negative band at 248 nm were still observed, while the positive band at 223 nm was replaced by the emerging negative band at 215 nm.[47] Figure 1 shows the CD

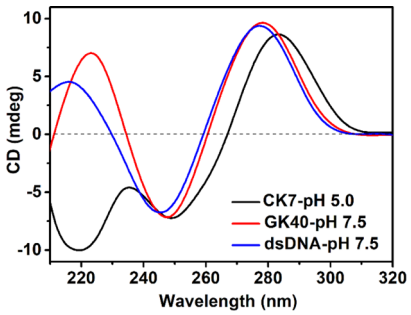

Figure 1. CD spectra for the antiparallel triplex GK40, parallel triplex CK7, and target duplex formed in 100 mM sodium phosphate buffer solution.

spectra measured here for the antiparallel triplex GK40, parallel triplex CK7, and their target duplex at room temperature, which are consistent with Fujimoto's results and demonstrate the formation of the anticipated triplex structures. In the triplex (GK40 or CK7), one-electron oxidation should take place preferentially on the GGC or C^+GC motifs containing G bases, whereas the AAT or TAT motifs cannot compete because G has the lowest oxidation potential. Thus, the $G^{\bullet+}$ degradation pathways in the antiparallel and parallel triplex can be monitored as follows.

Guanine Radical Cation Deprotonation in the Antiparallel Triplex. To assist in understanding the $G^{\bullet+}$ deprotonation in triplex DNA, a reference experiment was first performed for the one-electron oxidation of the target duplex by the $SO_4^{\bullet-}$ radical. $G^{\bullet+}$ in dsDNA is known to deprotonate N_1–H, forming $G(N_1–H)^{\bullet}$.[13,14] The transient absorption spectra for the 355 nm photolysis of the target duplex with $Na_2S_2O_8$ (Figure 2a) show the $SO_4^{\bullet-}$ band at 450 nm as well as the $G^{\bullet+}$ bands at 400 and 490 nm at 50 ns, which decay to form $G(N_1–H)^{\bullet}$. The spectrum at 10 μs shows the typical $G(N_1–H)^{\bullet}$ features of two resolved bands at 390 and 510 nm as well as flat absorption above 600 nm. To obtain the deprotonation rate constant, the absorption change of 640 nm where the deprotonated radical mainly absorbs was measured, which can be fit well by a biexponential function involving a fast increasing phase and a slow one. This is in accord with previous studies on the $G^{\bullet+}$ deprotonation in the duplex, in

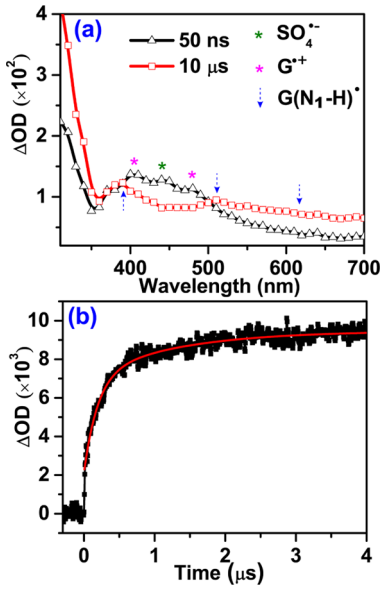

Figure 2. (a) Transient UV–vis absorption spectra for the buffer solution (pH = 7.5) of dsDNA (1.25 mM, the equivalent G-base concentration [G] = 5.0 mM) + $Na_2S_2O_8$ (400 mM) upon 355 nm laser flash photolysis. (b) Kinetics trace monitored at 640 nm after excitation of (a) solution, with the double-exponential fits to the data (solid red line).

which the fast phase was assigned to the bimolecular reaction of $SO_4^{\bullet-}$ with the duplex because rate constants increased with the concentration of the duplex, and the slower phase was considered to derive from the first-order $G^{\bullet+}$ deprotonation because of the independence on the duplex concentration.[13,14] In our case, the two time constants obtained from the 640 nm kinetics curve are 0.12 and 1.06 μs corresponding to oxidation and deprotonation, respectively. Here, the deprotonation rate is much slower than the oxidation rate, such that these two processes can be resolved directly from the 640 nm kinetics curves. The deprotonation rate constant is thus obtained to be $(9.4 \pm 0.5) \times 10^5\ s^{-1}$ for the target duplex.

For the antiparallel triplex containing G_2G_1C motifs, as shown in Scheme 2, G_2 in the third strand (G_2G_1C) is bound to the normal Watson–Crick base pair G_1C via the reverse Hoogsteen hydrogen bond. In the triplex G_2G_1C base pair under the attack of $SO_4^{\bullet-}$ radicals, which G base is more susceptible to oxidation? The electronic configuration of G_2G_1C was calculated at the level of PCM/B3LYP/6-31++G(d,p). It is noteworthy that almost all of the highest occupied molecular orbital (HOMO) of G_2G_1C is concentrated on G_2 (Figure 3a). This indicates that the hole ($G^{\bullet+}$) is preferentially localized on G_2 in the third strand, after the initial oxidation of the triplex. The subsequent deprotonation of $G^{\bullet+}$ could generate $G(N_1–H)^{\bullet}$ or $G(N_2–H)^{\bullet}$, depending on which the proton is to be released, the imino N_1–H or exocyclic amino N_2–H (Scheme 1).[14,15,48]

For the one-electron oxidation of the antiparallel triplex GK40 by $SO_4^{\bullet-}$, the transient absorption spectra (Figure 3b) show four peaks at 400, 450, 500, and 640 nm at early time (50 ns). The 450 nm band is due to $SO_4^{\bullet-}$, and the bands at 400 and 500 nm are the typical spectral position of $G^{\bullet+}$. With the decay of $G^{\bullet+}$, the transient bands of 390 and 510 nm are observed (10 μs, Figure 3b), along with a broad absorption band above 510 nm, which are the typical features for $G(N_1–H)^{\bullet}$.[13,14] On top of the broad absorption band above 510 nm,

DOI: 10.1021/acs.jpcb.9b00608
J. Phys. Chem. B 2019, 123, 2853–2863

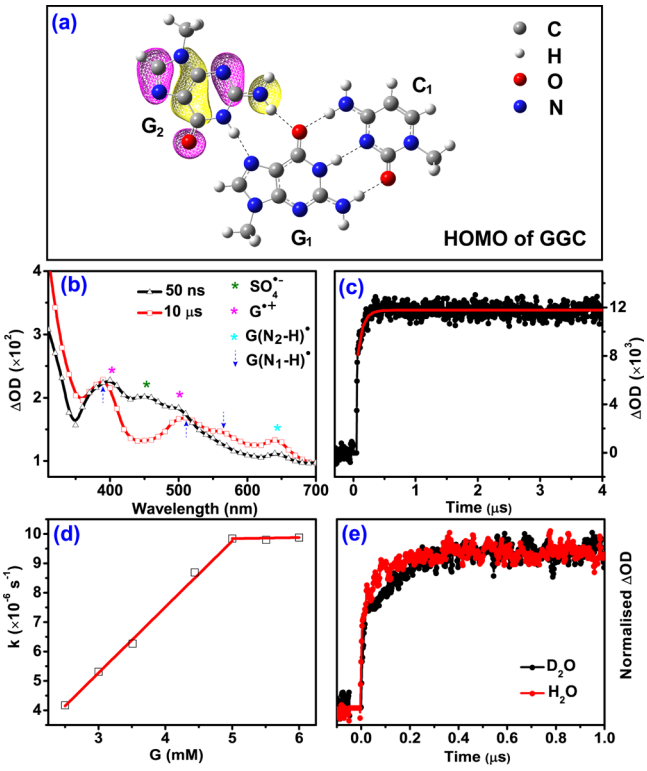

Figure 3. (a) Orbital contour plot of the HOMO of GGC obtained by the density functional calculation at the PCM/B3LYP/6-31++G(d,p) level. (b) Transient UV−vis absorption spectra for the buffer solution (pH=7.5) of the triplex GK40 ([G] = 5.0 mM) + $Na_2S_2O_8$ (400 mM) upon 355 nm laser flash photolysis. (c) Kinetics trace monitored at 640 nm after excitation of (b) solution, with the single-exponential fits to the data (solid red line). (d) Concentration dependence for the rate constants obtained from the increase of the 640 nm band. (e) Normalized kinetics traces at 640 nm after excitation of (b) in H_2O or in D_2O at pH/pD 7.5.

there is a small peak at 640 nm discerned. This is evidently different from the target duplex DNA. According to the literature, the absorption peak at ~620 nm is regarded to be specific for $G(N_2-H)^•$ and used to distinguish $G(N_2-H)^•$ from $G(N_1-H)^•$.[15,48,49] Thus, the 640 nm peak here can be attributed to the $G^{•+}$ deprotonation to form the neutral radical, $G(N_2-H)^•$. Because both $G(N_1-H)^•$ and $G(N_2-H)^•$ radicals are observed, the $G^{•+}$ deprotonation in the antiparallel triplex should occur at both the N_1-H and N_2-H sites, releasing both imino and amino protons.

The emergence of N_2-H deprotonation in addition to N_1-H deprotonation for $G^{•+}$ in the antiparallel triplex is a behavior distinct from its target duplex. To compare further, the deprotonation rate constant of $G^{•+}$ in the antiparallel triplex was measured by monitoring the kinetics traces at 640 nm. Unlike the target duplex, there is only one fast rising phase observed here, indicating that the $G^{•+}$ deprotonation is as fast and thus not resolved from the $SO_4^{•-}$ + G oxidation. To discriminate $G^{•+}$ deprotonation from one-electron oxidation, the G concentration dependence of the rate constant was assessed through varying the G concentration from 2.5 to 6.0 mM in the triplex GK40. As shown in Figure 3d, the rate constants obtained from the single-exponential fitting to the rising curves at 640 nm are plotted against the concentration of G in the triplex, which exhibits a linear relationship below 5.0 mM. Therefore, below 5.0 mM, the rate-determining step is the second-order oxidizing reaction of $SO_4^{•-}$ + G in the triplex GK40. From the slope, the second-order oxidation rate constant is calculated to be $(2.2 \pm 0.3) \times 10^9$ M^{-1} s^{-1}, which follows pseudo-first-order conditions because the concentration of G bases in the triplex is in large excess relative to $SO_4^{•-}$. The rate constants above 5.0 mM are independent of G concentration, indicating that the rate-determining step is the first-order $G^{•+}$ deprotonation, from which the deprotonation rate constant of $(9.8 \pm 0.2) \times 10^6$ s^{-1} is obtained. Moreover, the deprotonation rate constant was measured in H_2O and D_2O separately, from which the kinetic isotope effect (KIE) factor of (1.5 ± 0.1) can be obtained (Figure 3e).

We notice that the obtained deprotonation rate constant for the antiparallel triplex [$(9.8 \pm 0.2) \times 10^6$ s^{-1}] is much greater than that in the G-quadruplex (2.1×10^5 s^{-1}) and 1-methylguanosine (3.5×10^5 s^{-1}), where only the amino proton N_2-H is deprotonated.[15,48] In contrast, it is close to the rate constant of N_1-H deprotonation in free G (1.8×10^7 s^{-1} at pH 7.0)[13] and single-strand DNA (1.4×10^7 s^{-1} measured for the third-strand sequence at pH 7.5 as shown in Figure S1). This suggests that $G_2^{•+}$ in the third-strand of the triplex should mainly undergo N_1-H deprotonation, together with a small portion of N_2-H deprotonation (as featured by the weak absorption peak of $G(N_2-H)^•$ at 640 nm). Indeed, the kinetics traces at 560 nm due to $G(N_1-H)^•$ do not have much difference from that at 640 nm due to both $G(N_2-H)^•$ and $G(N_1-H)^•$ (Figure S2).

Generally, the $G^{•+}$ deprotonation is affected by the accessibility of water molecules, and the deprotonation site is closely associated with the proton surrounding.[13−15] For the free base dG and G in single-strand DNA, both N_1-H and N_2-H contact with bulk water directly. Thus, the deprotonation site is determined by the acidity of active protons, causing a preferential loss of N_1-H (pK_a = 3.9) rather than N_2-H (pK_a = 4.7).[13] In duplex DNA, the G base is paired with cytosine (C) through Watson−Crick hydrogen bonding. Because pK_a of N_3 in C (4.3) is higher than that of N_1 in $G^{•+}$ (3.9), the N_1 proton of $G^{•+}$ is transferred to N_3 of C in the base pair. The N_1-H deprotonation thus occurs along the central hydrogen bond in duplex DNA, and then, the proton is released into aqueous solution. In this case, the released N_1-H is a bound proton, and the deprotonation has a KIE factor of 3.8.[14]

For the antiparallel triplex, the third strand (purine-rich) binds in the major groove of the target duplex forming two new grooves, where there is the presence of long-resident water spines because of the unique positioning of the amino groups of the first-strand C and the third-strand G.[34,39] The spine of hydration brought by the third strand thus significantly alters the water accessibility. The active protons (N_1-H and N_2-H) of the oxidized G base (G_2) in the third strand, although Hoogsteen hydrogen bonded with G_1, could be exposed to water spines in the groove, rendering a strong interaction with water molecules directly. This situation is similar to the free base dG and single-strand DNA and can be evidenced by the almost same KIE factor of 1.5 typical for free protons (Figure 3e). The exposure to water spines may allow the loss of active protons from $G_2^{•+}$ directly into water. Under these circumstances, it is expected that the deprotonation of the imino proton N_1-H should be predominant because it is more acidic than the amino proton N_2-H. This analysis is in agreement with our experimental observation. Meanwhile, it should be

DOI: 10.1021/acs.jpcb.9b00608
J. Phys. Chem. B 2019, 123, 2853−2863

noticed that the imino proton N_1−H of $G_2^{\bullet+}$ is also bound with N_7 of G_1 by reverse Hoogsteen hydrogen bonding (Scheme 2), which is considered to be a weak hydrogen bonding with the low melting temperature (generally 30−40 °C) and easy to dissociate.[30,40] This means that when the imino proton N_1−H is deprotonated into bulk water, N_7 of G_1 would have an adverse effect by slightly hindering the proton escape. On the other hand, the amino protons N_2−H are less restricted because only N_2−H_a is hydrogen-bonded with O_6 of G_1 and the other proton N_2−H_b is free. Thus, the loss of the free amino proton N_2−H_b can compete with deprotonation of the imino proton N_1−H, as manifested by the observation of $G(N_2-H)^{\bullet}$ in the transient absorption spectra. Unlike the duplex, the bases in the third strand of the triplex should be more exposed to aqueous solution. The long-resident water spine in the triplex facilitates deprotonation, whereas the reverse Hoogsteen hydrogen bonding between G_2 and G_1 restricts the N_1−H proton. Consequently, the deprotonation rate for $G^{\bullet+}$ in the third strand of the antiparallel triplex becomes much faster than its target duplex, and there is an emergence of N_2−H deprotonation in addition to N_1−H deprotonation.

Guanine Radical Cation Deprotonation in the Parallel Triplex. For the parallel triplex CK7 which is formed under slightly acidic conditions (pH 5.0),[41,47] one-electron oxidation should take place on the C^+GC motifs containing the G base, where the C base in the third strand is protonated, and thus, Hoogsteen hydrogen bonded with G in the target duplex (denoted by $C_2^+G_1C_1$ in Scheme 2). The preferential hole localization in G can be confirmed by the electronic configuration calculation of $C_2^+G_1C_1$, which shows that the HOMO of $C_2^+G_1C_1$ is centered on G_1 (Figure 4a).

For the one-electron oxidation of the parallel triplex CK7 by $SO_4^{\bullet-}$, the transient spectra (Figure 4b) show the $SO_4^{\bullet-}$ band at 450 nm and $G^{\bullet+}$ bands at 400 and 490 nm at early time (50 ns). Accompanying with the decay of $G^{\bullet+}$, two resolved bands at 390 and 510 nm as well as flat absorption above 600 nm are observed as shown in the 10 μs spectrum, which is essentially similar to the spectra of $G_1(N_1-H)^{\bullet}$ obtained from its target duplex (Figure 2a), indicating that $G^{\bullet+}$ in the parallel triplex undergoes N_1−H deprotonation.

Similar to its target duplex, the transients at 640 nm in the triplex CK7 also involve a fast increase phase and a slow one (Figure 4c). The fast phase due to bimolecular oxidation reveals linear concentration dependence, and the slow phase corresponding to first-order deprotonation is insensitive to concentration (Figure 4d), from which the oxidation ($(1.7 \pm 0.2) \times 10^9$ M^{-1} s^{-1}) and deprotonation rate constant [$(6.0 \pm 0.3) \times 10^5$ s^{-1}] are derived, respectively. The deprotonation in the parallel triplex CK7 is slightly slower compared to its target duplex (9.4 ± 0.5) $\times 10^5$ s^{-1}. This should be caused by the acidic pH (5.0) under this circumstance for forming the triplex. As shown in Figure 4e, the deprotonation rate constant was measured in H_2O and D_2O separately. The KIE factor measured for the parallel triplex (3.3 ± 0.1) is similar to that of the duplex (3.8), indicating further that it is the bound N_1−H proton within G_1C_1 to be released. Overall, the $G^{\bullet+}$ deprotonation behavior for $C_2^+G_1C_1$ is similar to its target duplex G_1C_1, the presence of the third strand does not change deprotonation much.

Our observation of $G^{\bullet+}$ deprotonation in both the antiparallel and parallel triplex helix provides key knowledge of kinetics rate constants, which can rationalize previous

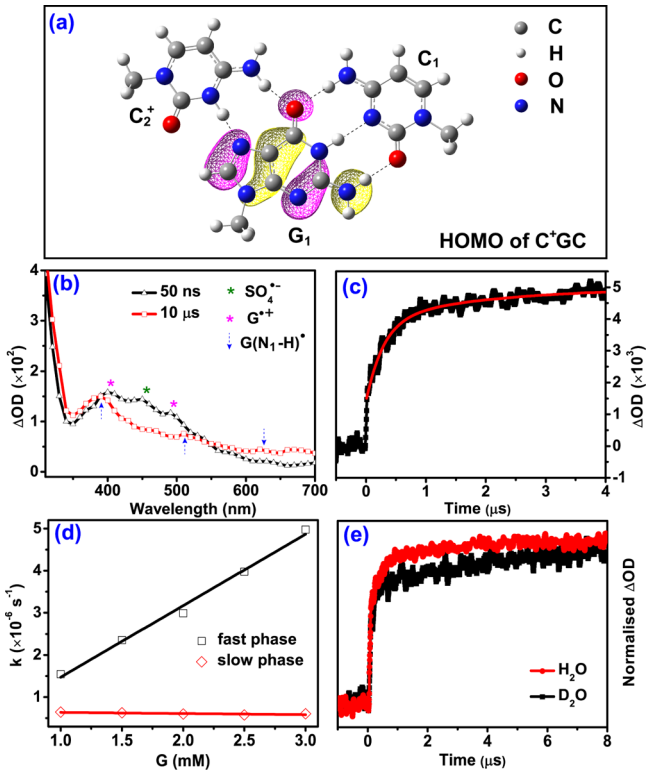

Figure 4. (a) Orbital contour plot of the HOMO of C^+GC obtained by the density functional calculation at the PCM/B3LYP/6-31++G(d,p) level. (b) Transient UV−vis absorption spectra for the buffer solution (pH = 5.0) of the triplex CK7 ([G] = 3.0 mM) + $Na_2S_2O_8$ (400 mM) upon 355 nm laser flash photolysis; (c) kinetics trace monitored at 640 nm after excitation of (b) solution, with the double-exponential fits to the data (solid line). (d) Concentration dependence for the rate constants obtained from the fast and slow increase phases of the 640 nm band. (e) Normalized kinetics traces at 640 nm after excitation of (b) in H_2O or in D_2O at pH/pD 5.0.

steady-state measurements of hole transfer in triplex DNA. The GGC in the antiparallel triplex is a more effective hole sink than the GGG triplet in the duplex based on the calculated ionization potential, and the hole prefers to localize on the triplex helix rather than the duplex.[40] This affords a prerequisite factor for the hole trap in this region. In addition, if the ensuing $G^{\bullet+}$ deprotonation in this site could compete with hole migration, the hole would be trapped here and generate the damage product of Iz or Oz. In fact, the deprotonation rate constant of the antiparallel triplex [$(9.8 \pm 0.2) \times 10^6$ s^{-1}] is 10 times greater than that in the target duplex [$(9.4 \pm 0.5) \times 10^5$ s^{-1}]. In this regard, the antiparallel triplex helix region is a preferential site for the hole trap compared to the duplex. Therefore, according to the ionization potential and deprotonation rate constants, it is understandable why the antiparallel triplex can serve as an effective hole trap and eventually result in the strand break related Iz and Oz lesions.[40] For the parallel triplex, the increased positive charge caused by the N_3 protonation of the C base in the third strand would raise the ionization potential of the $C_2^+G_1C_1$ unit in comparison with the GC base pair. This is disadvantageous for the initial hole localization in the parallel triplex. Furthermore, the slower deprotonation of $G^{\bullet+}$ in the parallel triplex [$(6.0 \pm 0.3) \times 10^5$ s^{-1}] would have less interruption on the hole transfer than that in the duplex. This accounts for why the parallel triplex region could block the hole trap and

DOI: 10.1021/acs.jpcb.9b00608
J. Phys. Chem. B 2019, 123, 2853−2863

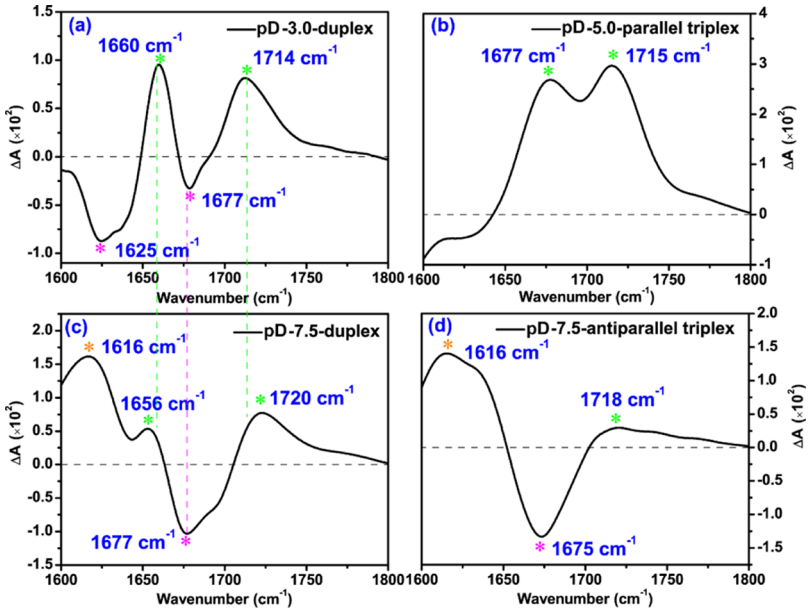

Figure 5. Steady-state IR difference spectra for (a) target duplex ([G] = 5.0 mM) + $Na_2S_2O_8$ (400 mM) at pD 3.0; (b) parallel triplex ([G] = 5.0 mM) + $Na_2S_2O_8$ (400 mM) at pD 5.0; (c) target duplex ([G] = 5.0 mM) + $Na_2S_2O_8$ (400 mM) at pD 7.5; and (d) antiparallel triplex ([G] = 5.0 mM) + $Na_2S_2O_8$ (400 mM) at pD 7.5 after 90 s of 355 nm laser irradiation.

Table 1. B3LYP/6-31++G(d,p) calculated IR Frequencies under the PCM Model or under the Solvent Model (Explicit Water + PCM) for G, G(+H)$^+$, 8-oxoG, and 5-HOO−(G−H) hydroperoxide in Duplex or Triplex Base Pairs

structure	In the base pair of	Vib. mode	ν_{cal} (cm^{-1}) under PCM	ν_{cal} (cm^{-1}) 7 water + PCM	ν_{exp} (cm^{-1})
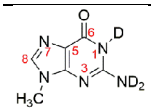 G	-	C6=O	1704	1671	1666
	G:C	C6=O	1668	1670	1677
	C^+:G:C	C6=O	1661	1665	-
	G:G:C	C6=O	1682	1670	1675
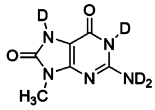 8-oxoG	G:C	C6=O	1666	1666	1660
		C8=O	1735	1730	1714
	C^+:G:C	C6=O	1668	1659	1677
		C8=O	1728	1718	1715
	G:G:C	C6=O	1672	1656	-
		C8=O	1733	1713	1718
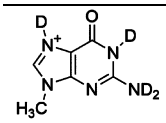 G(+H)$^+$	G:C	C6=O	1696	1687	-
		C4=C5	1636	1634	1625
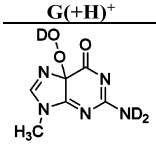 5-HOO-G(-H) hydroperoxide	-	N8=C7	1626	1636	1616
		C6=O	1697	1685	-

facilitate hole migration, featuring that the oxidative strand break occurred at remote GG locations.[41]

Guanine Radical Cation Hydration in Triplex DNA. Aside from deprotonation, $G^{\bullet+}$ can undergo hydration to form 8-oxoG by nucleophilic addition of water to C_8 of the guanine imidazole ring (Scheme 1). However, hydration occurs slowly at ~3 ms (3.0×10^2 s^{-1}),[25] which is beyond the time window of transient spectroscopy. The steady-state FTIR measurements were performed to monitor the hydration product 8-oxoG in triplex DNA, taking advantage of the characteristic IR bands in discerning the in-plane double-bond stretching vibrations (1600−1800 cm^{-1}). Brief laser irradiation (usually 90 s) was performed to avoid successive photo-absorption and reactions of primary products.

The reference experiment was first performed for the target duplex. As $G^{\bullet+}$ in duplex DNA decays by both the deprotonation and hydration in neutral pH conditions, the deprotonation products may interfere with the measurement of

DOI: 10.1021/acs.jpcb.9b00608
J. Phys. Chem. B 2019, 123, 2853−2863

8-oxoG formation. To obtain the characteristic IR spectra of the hydration product 8-oxoG, the experiment was carried out at pD 3.0 in deuterium oxide, where deprotonation is suppressed and $G^{\bullet+}$ can only hydrate to form 8-oxoG. Figure 5a shows the IR difference spectra after 355 nm laser irradiation (90 s) of the mixed solution of the target duplex and $Na_2S_2O_8$ at pD 3.0. Strong IR bands due to the reaction of G + $SO_4^{\bullet-}$ are observed, where the depletion of the reactant (G) gives rise to negative signals and the formation of products corresponds to positive bands. The two negative peaks at 1625 and 1677 cm^{-1} should be ascribed to G bleach. To assist assignment, the IR frequencies of G in the GC base pair were calculated at the level of B3LYP/6-31++G(d,p). Considering the rapid exchange of hydrogens by deuterons in D_2O solution, both imino and amino protons in G are replaced by deuterons in the calculation. The solvent effects were simulated with the PCM or under the solvent model that includes seven explicit water molecules (D_2O) combined with a PCM approach. The calculated vibrational frequencies based on the approach of (explicit water + PCM) are in better agreement with the experimental IR absorption spectra in general (Table 1). According to the calculations, the 1677 cm^{-1} band in IR difference spectra should be assigned to the C6═O carbonyl stretching mode of G (calculated IR frequency at 1670 cm^{-1}). At acidic pH (3.0), G can be partially protonated at the N_7 site (pK_a=2.4). Thus, the other negative band at 1625 cm^{-1} should be ascribed to the protonated G (G(+H)$^+$), which agrees with the calculated IR frequency of 1634 cm^{-1} for the C4═C5 stretching mode of G(+H)$^+$.

The G bleach bands are accompanied by the formation of two obvious positive bands at 1660 and 1714 cm^{-1} in the IR difference spectra (Figure 5a). These positive bands should be ascribed to the formation of 8-oxoG. The IR frequencies for 8-oxoG in the GC base pair were also calculated to confirm the assignment. The calculated IR frequencies of 8-oxoG at 1666 (C6═O carbonyl stretching mode) and 1730 cm^{-1} (C8═O carbonyl stretching mode) are consistent with the experimental observation. The agreement between the calculation and the experiment supports the assignment of the hydration product 8-oxoG in the duplex. The standard IR spectra for G and 8-oxoG can thus be obtained, which are featured with the band at 1677 cm^{-1} for G depletion and two bands at 1660 and 1714 cm^{-1} for 8-oxoG.

In contrast, in neutral conditions at pD 7.5 for the target duplex, the IR difference spectrum (Figure 5c) displays different features. Together with the negative band due to G bleach at 1677 cm^{-1}, three positive bands at 1616, 1656, and 1720 cm^{-1} are observed. Among them, the bands at 1656 and 1720 cm^{-1} are the standard IR spectra for 8-oxoG. In neutral conditions because both hydration and deprotonation occur, the other positive band at 1616 cm^{-1} should be ascribed to the deprotonation product. It was proposed that the deprotonated radical G(−H)$^\bullet$ reacts with O_2 ($<10^6$ M^{-1} s^{-1}, ∼ ms at the saturated O_2 concentration of 0.3 mM) to form the hydroperoxide 5-HOO−(G−H), by addition of O_2 to C_5 of G(−H)$^\bullet$.[50] As shown in Scheme 1, the hydroperoxide then undergoes decarboxylation, ring-opening, hydrolysis, and ring-chain tautomerization to form eventually Iz and Oz lesion products, which, however, should occur much more slowly. Thus, the 1616 cm^{-1} product detected in the IR spectra after 90 s of laser irradiation most likely arises from the fast radical reaction (G(−H)$^\bullet$ + O_2) product 5-HOO−(G−H) hydroperoxide. The calculated frequency for the N7═C8 stretching mode of 5-HOO−(G−H) is 1626 cm^{-1} under the PCM model or 1636 cm^{-1} under the (explicit water + PCM) model, which matches with the experiment and confirms the assignment. The C6═O mode of 5-HOO−(G−H) (calculated frequency 1685 cm^{-1}) should be buried inside the negative G bleach band and thus not discernible. The other products formed subsequent to hydroperoxide do not have IR absorption in this region. The IR spectra thus verify the previously postulated hydroperoxide intermediate product prior to the formation of Iz and Oz lesions. It is noticeable that the intensity of the 8-oxoG band is weaker than in pD 3.0 conditions, indicating that hydration is less competitive at pD 7.5. These results corroborate previous studies that $G^{\bullet+}$ in duplex DNA at neutral pH decays by both deprotonation and hydration.[21]

Similar experiments were performed for triplex DNA of the parallel triplex CK7 and antiparallel triplex GK40, and the IR difference spectra are shown in Figure 5b,d. Interestingly, for the parallel triplex CK7, two strong positive bands at 1677 and 1715 cm^{-1} are observed, which are the standard IR frequencies for 8-oxoG, indicating that $G^{\bullet+}$ undergoes hydration to generate 8-oxoG. The intensity of the 8-oxoG band here is ∼3 fold stronger than that in the target dsDNA (pD 3.0), indicating the much larger product yields of 8-oxoG in the parallel triplex. This can be evidenced further by the absence of the negative peak associating with the G bleach, which should be buried by the strong positive peaks of 8-oxoG. The calculated C6═O IR frequency of G (1665 cm^{-1}) in C^+GC does not differ much from 8-oxoG (1659 cm^{-1}) in C^+GC as shown in Table 1, which further confirms that the negative band of G overlaps with the positive band of 8-oxoG. This overlapping makes the intensity of C6═O at 1677 cm^{-1} less strong than that of C8═O at 1715 cm^{-1}. Aside from 8-oxoG, there is no $G^{\bullet+}$ deprotonation product observed, which should have the IR band at ∼1616 cm^{-1}, indicating that $G^{\bullet+}$ deprotonation in the parallel triplex is negligible comparing with $G^{\bullet+}$ hydration. The IR results fully corroborate the observations in transient UV−vis spectra. The main reason for the dominant hydration pathway and much greater 8-oxoG product yield than the target duplex can be speculated: (i) more cationic character retained for the guanine radical because of the protonation of C in the third strand, which is Hoogsteen hydrogen bond with G and (ii) the slower deprotonation rate of $G^{\bullet+}$, which may make hydration to effectively compete with deprotonation.

In contrast, for the antiparallel triplex GK40 (Figure 5d), there are one negative band and two positive bands (one strong band at 1616 cm^{-1} and one weak band at 1718 cm^{-1}) in the IR difference spectra. The negative peaks at 1675 cm^{-1} are basically consistent with the standard IR spectra for G and the calculated IR frequency (1670 cm^{-1}) for G in $G_2G_1C_1$ of the antiparallel triplex. The strong positive band at 1616 cm^{-1} should arise from the 5-HOO−(G−H) hydroperoxide formed after $G^{\bullet+}$ deprotonation, with the same IR frequency as that in the target duplex when deprotonation occurs (pD 7.5). The weak positive band at 1718 cm^{-1} should be 8-oxoG, which apparently has negligible product yields such that the other band of 8-oxoG at 1660 cm^{-1} is buried inside the negative band of G at 1675 cm^{-1} and thus not discernible. The calculative IR frequencies (Table 1) also confirm these assignments. The trace amounts of the 8-oxoG formation in the antiparallel triplex are concomitant with the much larger product yield of 5-HOO−(G−H) hydroperoxide from deprotonation, corroborating that the long-residence water in

DOI: 10.1021/acs.jpcb.9b00608
J. Phys. Chem. B 2019, 123, 2853−2863

the third strand facilitates $G^{\bullet+}$ deprotonation and thus hydration cannot compete with the fast deprotonation.

Here, our results reveal that the decay pathways of $G^{\bullet+}$ in the triplex differ from that in the duplex, and there is a pronounced structural effect on the reactivity. For the antiparallel triplex, G in the third strand (G_2) is paired with the G base in the target duplex (G_1) by the reverse Hoogsteen hydrogen bond. This structure renders larger water accessibility because of long residence of water spines, which makes $G_2^{\bullet+}$ undergo deprotonation by loss of both imino and amino protons directly into bulk water and $G(-H)^{\bullet}$ would not retain any cationic character. Thus, $G^{\bullet+}$ in the antiparallel triplex decays primarily by deprotonation and would eventually lead to the strand break related Iz and Oz lesion products. However, $G^{\bullet+}$ in the parallel triplex ($G_1^{\bullet+}$) locates in the target duplex, and the active protons (imino and amino proton) of $G_1^{\bullet+}$ have almost a similar hydrogen bonding structure with that in duplex DNA. This structural features cause $G(-H)^{\bullet}$ in the parallel triplex retaining some cationic character, and the diminishing probability of escape of the proton due to intrabase-pair proton equilibrium of $[G(-H)^{\bullet}:H^{+}C \leftrightarrows G^{\bullet+}:C]$. It is also noteworthy that $G_1^{\bullet+}$ is paired with the protonated C base locating in the third strand, which would lead to more cationic character of $G(-H)^{\bullet}$ in comparison with the duplex. In this regard, the hydration of $G^{\bullet+}$ in the parallel triplex should be more effective. As manifested by the IR difference spectra, the dominant decay pathway of $G^{\bullet+}$ in the parallel triplex is hydration, leading to the 8-oxoG type of damage. These results clearly show that the degradation pathways of $G^{\bullet+}$ are highly sensitive to DNA structures.

CONCLUSIONS

In this work, the structure-dependent reaction pathways of $G^{\bullet+}$ in both parallel and antiparallel triplex DNA are unveiled by time-resolved UV−vis and steady-state FTIR spectroscopy. For the antiparallel triplex with the GGC motif, $G^{\bullet+}$ mainly undergoes fast deprotonation $(9.8 \pm 0.2) \times 10^6\ s^{-1}$, releasing both N_1−H and N_2−H of G in the third strand directly into bulk water. The unique deprotonation behavior should be related to the presence of the long-resident water spines brought by the third strand, which can facilitate the release of protons directly to water, and the deprotonation rate constant is even higher than that in the target duplex $[(9.4 \pm 0.5) \times 10^5\ s^{-1}]$. Accordingly, $G^{\bullet+}$ hydration cannot compete with deprotonation, leading to negligible product yield of 8-oxo-G in the antiparallel triplex. Instead, the 5-HOO−(G−H) hydroperoxide formed after $G^{\bullet+}$ deprotonation is identified in the IR spectra. In contrast, in the parallel triplex with the C^{+}GC motif, the deprotonation of $G^{\bullet+}$ behaves similarly with the target duplex by releasing only N_1−H and occurs more slowly $(6.0 \pm 0.3) \times 10^5\ s^{-1}$ because of the slightly acidic pH (5.0), while $G^{\bullet+}$ hydration becomes the major pathway with yields of 8-oxo-G larger than in the duplex (pH 3.0). The increased positive charge brought by the third strand makes the G radical in the parallel triplex sustain more cation character and prone for hydration. These results reveal the significant roles of the DNA structure in governing $G^{\bullet+}$ reaction dynamics and decay pathways.

The initial reaction pathways of $G^{\bullet+}$ revealed here indicate that one-electron oxidation of triplex DNA can incur severe chemical alterations, that is, prone hydration of $G^{\bullet+}$ in the parallel triplex leads to the 8-oxoG lesion, while the dominant $G^{\bullet+}$ deprotonation in the antiparallel triplex can be converted to Iz and Oz lesion-type causing strand breaks. In terms of these deleterious oxidation reactions, it can be understood why non-B DNA such as the triplex can be more susceptible to DNA damage than the canonical B-DNA structure. It was observed that UV irradiation caused significant chromatin fragmentation at repetitive sequences in mammalian cells, particularly at homopurine/homopyrimidine regions that can fold into the intramolecular triplex.[43] It was not clear whether the accumulated mutations were caused by higher levels of UV damage in the non-B DNA-forming sequences or because of a lower repair efficiency in the structured regions, or both. The results here indicate that non-B DNA (triplex) plays an important role in DNA damage formation and provide mechanistic insights to rationalize why the genomic regions with the propensity to fold transiently into non-B DNA secondary structures can become hot spots for mutagenesis.

ASSOCIATED CONTENT

Supporting Information

The Supporting Information is available free of charge on the ACS Publications website at DOI: 10.1021/acs.jpcb.9b00608.

Additional kinetics data (PDF)

AUTHOR INFORMATION

Corresponding Author

*E-mail: hongmei@bnu.edu.cn.

ORCID

Hongmei Su: 0000-0001-7384-6523

Notes

The authors declare no competing financial interest.

ACKNOWLEDGMENTS

This work was financially supported by the National Natural Science Foundation of China (grant nos. 21425313, 21727803, 21773013, and 21773257).

REFERENCES

(1) Dizdaroglu, M. Oxidatively Induced DNA Damage and Its Repair in Cancer. *Mutat. Res., Rev. Mutat. Res.* **2015**, *763*, 212−245.

(2) Whitaker, A. M.; Schaich, M. A.; Smith, M. S.; Flynn, T. S.; Freudenthal, B. D. Base Excision Repair of Oxidative DNA Damage: from Mechanism to Disease. *Front. Biosci.* **2017**, *22*, 1493−1522.

(3) Jie, J.; Liu, K.; Wu, L.; Zhao, H.; Song, D.; Su, H. Capturing the Radical Ion-Pair Intermediate in DNA Guanine Oxidation. *Sci. Adv.* **2017**, *3*, No. e1700171.

(4) Ding, H.; Greenberg, M. M. Hole Migration is the Major Pathway Involved in Alkali-Labile Lesion Formation in DNA by the Direct Effect of Ionizing Radiation. *J. Am. Chem. Soc.* **2007**, *129*, 772−773.

(5) Cadet, J.; Wagner, J. R.; Shafirovich, V.; Geacintov, N. E. One-electron Oxidation Reactions of Purine and Pyrimidine Bases in Cellular DNA. *Int. J. Radiat. Biol.* **2014**, *90*, 423−432.

(6) Wang, Y.; Zhao, H.; Yang, C.; Jie, J.; Dai, X.; Zhou, Q.; Liu, K.; Song, D.; Su, H. Degradation of Cytosine Radical Cations in 2′-Deoxycytidine and in i-Motif DNA: Hydrogen-Bonding Guided Pathways. *J. Am. Chem. Soc.* **2019**, *141*, 1970−1979.

(7) Morikawa, M.; Kino, K.; Oyoshi, T.; Suzuki, M.; Kobayashi, T.; Miyazawa, H. Product analysis of photooxidation in isolated quadruplex DNA; 8-oxo-7,8-dihydroguanine and its oxidation product at 3′-G are formed instead of 2,5-diamino-4H-imidazol-4-one. *RSC Adv.* **2013**, *3*, 25694−25697.

(8) Fleming, A. M.; Burrows, C. J. G-Quadruplex Folds of the Human Telomere Sequence Alter the Site Reactivity and Reaction

DOI: 10.1021/acs.jpcb.9b00608
J. Phys. Chem. B 2019, 123, 2853−2863

Pathway of Guanine Oxidation Compared to Duplex DNA. *Chem. Res. Toxicol.* **2013**, *26*, 593−607.
(9) Morikawa, M.; Kino, K.; Oyoshi, T.; Suzuki, M.; Kobayashi, T.; Miyazawa, H. Analysis of Guanine Oxidation Products in Double-Stranded DNA and Proposed Guanine Oxidation Pathways in Single-Stranded, Double-Stranded or Quadruplex DNA. *Biomolecules* **2014**, *4*, 140.
(10) Bezzina, J. P.; Prendergast, M. B.; Blanksby, S. J.; Trevitt, A. J. Gas-Phase Oxidation of the Protonated Uracil-5-yl Radical Cation. *J. Phys. Chem. A* **2018**, *122*, 890−896.
(11) Cadet, J.; Davies, K. J. A.; Medeiros, M. H. G.; Di Mascio, P.; Wagner, J. R. Formation and Repair of Oxidatively Generated Damage in Cellular DNA. *Free Radical Biol. Med.* **2017**, *107*, 13−34.
(12) Ravanat, J.-L.; Douki, T. UV and Ionizing Radiations Induced DNA Damage, Differences and Similarities. *Radiat. Phys. Chem.* **2016**, *128*, 92−102.
(13) Kobayashi, K.; Tagawa, S. Direct Observation of Guanine Radical Cation Deprotonation in Duplex DNA Using Pulse Radiolysis. *J. Am. Chem. Soc.* **2003**, *125*, 10213−10218.
(14) Kobayashi, K.; Yamagami, R.; Tagawa, S. Effect of Base Sequence and Deprotonation of Guanine Cation Radical in DNA. *J. Phys. Chem. B* **2008**, *112*, 10752−10757.
(15) Wu, L.; Liu, K.; Jie, J.; Song, D.; Su, H. Direct Observation of Guanine Radical Cation Deprotonation in G-Quadruplex DNA. *J. Am. Chem. Soc.* **2015**, *137*, 259−266.
(16) Jena, N. R.; Mishra, P. C. Formation of Ring-Opened and Rearranged Products of Guanine: Mechanisms and Biological Significance. *Free Radical Biol. Med.* **2012**, *53*, 81−94.
(17) So, S.; Kirk, B. B.; Trevitt, A. J.; Wille, U.; Blanksby, S. J.; da Silva, G. Unimolecular Reaction Chemistry of a Charge-Tagged Beta-Hydroxyperoxyl Radical. *Phys. Chem. Chem. Phys.* **2014**, *16*, 24954−24964.
(18) Cadet, J.; Douki, T.; Ravanat, J.-L. Oxidatively Generated Damage to the Guanine Moiety of DNA: Mechanistic Aspects and Formation in Cells. *Acc. Chem. Res.* **2008**, *41*, 1075−1083.
(19) Burrows, C. J.; Muller, J. G. Oxidative Nucleobase Modifications Leading to Strand Scission. *Chem. Rev.* **1998**, *98*, 1109−1152.
(20) Armitage, B. Photocleavage of Nucleic Acids. *Chem. Rev.* **1998**, *98*, 1171−1200.
(21) Rokhlenko, Y.; Cadet, J.; Geacintov, N. E.; Shafirovich, V. Mechanistic Aspects of Hydration of Guanine Radical Cations in DNA. *J. Am. Chem. Soc.* **2014**, *136*, 5956−5962.
(22) Greenberg, M. M. The Formamidopyrimidines: Purine Lesions Formed in Competition With 8-Oxopurines from Oxidative Stress. *Acc. Chem. Res.* **2012**, *45*, 588−597.
(23) Bilotti, K.; Tarantino, M. E.; Delaney, S. Human Oxoguanine Glycosylase 1 Removes Solution Accessible 8-Oxo-7,8-dihydroguanine Lesions from Globally Substituted Nucleosomes Except in the Dyad Region. *Biochemistry* **2018**, *57*, 1436−1439.
(24) Pande, P.; Haraguchi, K.; Jiang, Y.-L.; Greenberg, M. M.; Basu, A. K. Unlike Catalyzing Error-Free Bypass of 8-OxodGuo, DNA Polymerase λ Is Responsible for a Significant Part of Fapy·dG-Induced G → T Mutations in Human Cells. *Biochemistry* **2015**, *54*, 1859−1862.
(25) Rokhlenko, Y.; Geacintov, N. E.; Shafirovich, V. Lifetimes and Reaction Pathways of Guanine Radical Cations and Neutral Guanine Radicals in an Oligonucleotide in Aqueous Solutions. *J. Am. Chem. Soc.* **2012**, *134*, 4955−4962.
(26) Bissler, J. J. Triplex DNA and Human Disease. *Front. Biosci.* **2007**, *12*, 4536−4546.
(27) Duca, M.; Vekhoff, P.; Oussedik, K.; Halby, L.; Arimondo, P. B. The Triple Helix: 50 Years Later, the Outcome. *Nucleic Acids Res.* **2008**, *36*, 5123−5138.
(28) Bacolla, A.; Wang, G. L.; Vasquez, K. M., New Perspectives on DNA and RNA Triplexes As Effectors of Biological Activity. *PLoS Genet.*. **2015**, *11*. DOI: 10.1371/journal.pgen.1005696
(29) Rajeswari, M. R. DNA triplex structures in neurodegenerative disorder, Friedreich's ataxia. *J. Biosci.* **2012**, *37*, 519−532.
(30) Walsh, S.; El-Sagheer, A. H.; Brown, T. Fluorogenic Thiazole Orange TOTFO Probes Stabilise Parallel DNA Triplexes at pH 7 and above. *Chem. Sci.* **2018**, *9*, 7681−7687.
(31) Ren, J.; Hu, Y.; Lu, C.-H.; Guo, W.; Aleman-Garcia, M. A.; Ricci, F.; Willner, I. pH-Responsive and Switchable Triplex-Based DNA Hydrogels. *Chem. Sci.* **2015**, *6*, 4190−4195.
(32) Boehm, B. J.; Whidborne, C.; Button, A. L.; Pukala, T. L.; Huang, D. M. DNA Triplex Structure, Thermodynamics, and Destabilisation: Insight from Molecular Simulations. *Phys. Chem. Chem. Phys.* **2018**, *20*, 14013−14023.
(33) Shields, G. C.; Laughton, C. A.; Orozco, M. Molecular Dynamics Simulations of the d(T·A·T) Triple Helix. *J. Am. Chem. Soc.* **1997**, *119*, 7463−7469.
(34) Mohan, V.; Smith, P. E.; Pettitt, B. M. Evidence for a New Spine of Hydration: Solvation of DNA Triple Helixes. *J. Am. Chem. Soc.* **1993**, *115*, 9297−9298.
(35) Arcella, A.; Portella, G.; Ruiz, M. L.; Eritja, R.; Vilaseca, M.; Gabelica, V.; Orozco, M. Structure of Triplex DNA in the Gas Phase. *J. Am. Chem. Soc.* **2012**, *134*, 6596−6606.
(36) Radhakrishnan, I.; Patel, D. J. Solution structure of a purine·purine·pyrimidine DNA triplex containing G·GC and T·AT triples. *Structure* **1993**, *1*, 135−152.
(37) Thenmalarchelvi, R.; Yathindra, N. New Insights into DNA Triplexes: Residual Twist and Radial Difference as Measures of Base Triplet Non-Isomorphism and their Implication to Sequence-Dependent Non-Uniform DNA Triplex. *Nucleic Acids Res.* **2005**, *33*, 43−55.
(38) Radhakrishnan, I.; Patel, D. J. Solution structure of a pyrimidine·purine·pyrimidine DNA triplex containing T·AT, C+ · GC and G·TA triples. *Structure* **1994**, *2*, 17−32.
(39) Mohan, V.; Smith, P. E.; Pettitt, B. M. Molecular Dynamics Simulation of Ions and Water around Triplex DNA. *J. Phys. Chem.* **1993**, *97*, 12984−12990.
(40) Dohno, C.; Nakatani, K.; Saito, I. Guanine of the Third Strand of C·G*G Triplex Serves as an Effective Hole Trap. *J. Am. Chem. Soc.* **2002**, *124*, 14580−14585.
(41) Kan, Y.; Schuster, G. B. Radical Cation Transport and Reaction in Triplex DNA: Long-Range Guanine Damage. *J. Am. Chem. Soc.* **1999**, *121*, 11607−11614.
(42) Wang, G.; Vasquez, K. M. Impact of Alternative DNA Structures on DNA Damage, DNA Repair, and Genetic Instability. *DNA Repair* **2014**, *19*, 143−151.
(43) Wang, G.; Vasquez, K. M. Models for Chromosomal Replication-Independent Non-B DNA Structure-Induced Genetic Instability. *Mol. Carcinog.* **2009**, *48*, 286−298.
(44) Zou, X.; Dai, X.; Liu, K.; Zhao, H.; Song, D.; Su, H. Photophysical and Photochemical Properties of 4-Thiouracil: Time-Resolved IR Spectroscopy and DFT Studies. *J. Phys. Chem. B* **2014**, *118*, 5864−5872.
(45) Bucher, D. B.; Pilles, B. M.; Pfaffeneder, T.; Carell, T.; Zinth, W. Fingerprinting DNA Oxidation Processes: IR Characterization of the 5-Methyl-2′-Deoxycytidine Radical Cation. *ChemPhysChem* **2014**, *15*, 420−423.
(46) Frisch, M. J.; Trucks, G. W.; Schlegel, H. B.; Scuseria, G. E.; Robb, M. A.; Cheeseman, J. R.; Scalmani, G.; Barone, V.; Mennucci, B.; Petersson, G. A.; Nakatsuji, H.; Caricato, M.; Li, X.; Hratchian, H. P.; Izmaylov, A. F.; Bloino, J.; Zheng, G.; Sonnenberg, J. L.; Hada, M.; Ehara, M.; Toyota, K.; Fukuda, R.; Hasegawa, J.; Ishida, M.; Nakajima, T.; Honda, Y.; Kitao, O.; Nakai, H.; Vreven, T.; Montgomery, J. A., Jr.; Peralta, J. E.; Ogliaro, F.; Bearpark, M.; Heyd, J. J.; Brothers, E.; Kudin, K. N.; Staroverov, V. N.; Kobayashi, R.; Normand, J.; Raghavachari, K.; Rendell, A.; Burant, J. C.; Iyengar, S. S.; Tomasi, J.; Cossi, M.; Rega, N.; Millam, J. M.; Klene, M.; Knox, J. E.; Cross, J. B.; Bakken, V.; Adamo, C.; Jaramillo, J.; Gomperts, R.; Stratmann, R. E.; Yazyev, O.; Austin, A. J.; Cammi, R.; Pomelli, C.; Ochterski, J. W.; Martin, R. L.; Morokuma, K.; Zakrzewski, V. G.; Voth, G. A.; Salvador, P.; Dannenberg, J. J.; Dapprich, S.; Daniels, A. D.; Farkas, O.; Foresman, J. B.; Ortiz, J. V.; Cioslowski, J.; Fox, D. J. *Gaussian 09*, Revision A.01; Gaussian, Inc.: Wallingford, CT, 2009.

DOI: 10.1021/acs.jpcb.9b00608
J. Phys. Chem. B 2019, 123, 2853−2863

(47) Fujimoto, K.; Yoshinaga, H.; Yoshio, Y.; Sakamoto, T. Quick and Reversible Photocrosslinking Reaction of 3-Cyanovinylcarbazole Nucleoside in a DNA Triplex. *Org. Biomol. Chem.* **2013**, *11*, 5065−5068.
(48) Candeias, L. P.; Steenken, S. Ionization of Purine Nucleosides and Nucleotides and their Components by 193-nm Laser Photolysis in Aqueous Solution: Model Studies for Oxidative Damage of DNA. *J. Am. Chem. Soc.* **1992**, *114*, 699−704.
(49) Adhikary, A.; Kumar, A.; Becker, D.; Sevilla, M. D. The Guanine Cation Radical: Investigation of Deprotonation States by ESR and DFT. *J. Phys. Chem. B* **2006**, *110*, 24171−24180.
(50) Candeias, L. P.; Steenken, S. Reaction of HO. with Guanine Derivatives in Aqueous Solution: Formation of Two Different Redox-Active OH-Adduct Radicals and Their Unimolecular Transformation Reactions. Properties of G(-H). *Chem.—Eur. J.* **2000**, *6*, 475−484.

DOI: 10.1021/acs.jpcb.9b00608
J. Phys. Chem. B 2019, 123, 2853−2863